



RESEARCH ARTICLE

WILEY

Autonomic flexibility reflects learning and associated neuroplasticity in old age

Quanjing Chen^{1,2} | Haichuan Yang³ | Brian Rooks^{1,4} | Mia Anthony^{1,5} | Zhengwu Zhang^{4,6} | Duje Tadin^{5,6} | Kathi L. Heffner^{1,2} | Feng V. Lin^{1,2,5,6,7}

¹Elaine C. Hubbard Center for Nursing Research on Aging, School of Nursing, University of Rochester Medical Center, Rochester, New York

²Department of Psychiatry, School of Medicine and Dentistry, University of Rochester Medical Center, Rochester, New York

³Department of Computer Science, University of Rochester, Rochester, New York

⁴Department of Biostatistics and Computational Biology, University of Rochester Medical Center, Rochester, New York

⁵Department of Brain and Cognitive Sciences, University of Rochester, Rochester, New York

⁶Department of Neuroscience, School of Medicine and Dentistry, University of Rochester Medical Center, Rochester, New York

⁷Department of Neurology, School of Medicine and Dentistry, University of Rochester Medical Center, Rochester, New York

Correspondence

Quanjing Chen and Feng V. Lin, CogT Lab, UR CABIN, 430 Elmwood Ave, Rochester, NY 14620.

Email: quanjing_chen@urmc.rochester.edu (Q. C.) and fengvankee_lin@urmc.rochester.edu (F. L.)

Funding information

NIH, Grant/Award Numbers: NR015452, R01

Abstract

Effective learning in old age, particularly in those at risk for dementia, is essential for prolonging independent living. Individual variability in learning, however, is remarkable; that is, months of cognitive training to improve learning may be beneficial for some individuals but not others. So far, little is known about which neurophysiological mechanisms account for the observed variability in learning induced by cognitive training in older adults. By combining Lövdén et al.'s (2010, A theoretical framework for the study of adult cognitive plasticity. *Psychological Bulletin*, 136, 659–676) framework proposing the role of adaptation capacity in neuroplasticity and a neurovisceral integration model of the relationship between autonomic nervous system (ANS) and brain with a novel shapelet analytical approach that allows for accurate and interpretable analysis of time series data, we discovered an acute, ECG-derived ANS segment in response to cognitive training tasks at baseline that predicted learning outcomes from a 6-week cognitive training intervention. The relationship between the ANS segment and learning was robust in both cross-participant and cross-task analyses among a group of older adults with amnesic mild cognitive impairment. Furthermore, the revealed ANS shapelet significantly predicted training-induced neuroplasticity in the dorsal anterior cingulate cortex and select frontal regions during task fMRI. Across outcome measures, individuals were less likely to prospectively benefit from the cognitive training if their ECG data were more similar to this particular ANS segment at baseline. Our findings are among the first empirical evidence to confirm that adaptation capacity, indexed by ANS flexibility, predicts individual differences in learning and associated neuroplasticity beyond individual characteristics (e.g., age, education, neurodegeneration, total training).

KEYWORDS

adaptation capacity, amnesic mild cognitive impairment, anterior cingulate cortex, autonomic nervous system, learning

Quanjing Chen and Haichuan Yang have contributed equally to this work.

This is an open access article under the terms of the Creative Commons Attribution-NonCommercial-NoDerivs License, which permits use and distribution in any medium, provided the original work is properly cited, the use is non-commercial and no modifications or adaptations are made.

© 2020 The Authors. *Human Brain Mapping* published by Wiley Periodicals, Inc.

1 | INTRODUCTION

It is vital to identify physiological factors contributing to “healthspan” in the aging process (Seals, Justice, & LaRocca, 2016). Effective learning in older age, especially in those at risk for dementia, is essential for prolonging independent living. Cumulative literature suggests that the capacity to learn endures despite old age or neurodegeneration (Lampit, Hallock, & Valenzuela, 2014; Lövdén, Backman, Lindenberger, Schaefer, and Schmiedek, 2010; Shao et al., 2015). Individual variability in learning, however, is remarkable; months of cognitive training aimed at improving learning may be beneficial for some individuals while inadequate for others (Lampit et al., 2014; Shao et al., 2015). Yet, we know very little about how to explain these differences in learning capacity, such as why some individuals, despite their effort, fail to benefit from cognitive training. In attempt to answer this question, we adopted and synthesized two frameworks, one proposing that adaptation capacity—the ability to respond flexibly to environmental demands—is a key contributor to neuroplasticity underlying broad and sustained effects of cognitive training (Lövdén et al., 2010) and the other—neurovisceral integration theory—emphasizing the relationship between the brain and autonomic nervous system (ANS) flexibility, an important indicator for adaptation capacity (Thayer & Lane, 2000). We hypothesized that individual differences in adaptation capacity, which can be monitored via ANS flexibility, will explain the variability in learning in old age.

According to the neurovisceral integration theory, ANS flexibility reflects the integrity of central and peripheral systems that support adaptation to environmental demands, thereby serving as a key indicator of and contributor to adaptation capacity (Thayer & Lane, 2000). There is an age-associated decline in ANS function, particularly in the parasympathetic branch; however, the difference in ANS function between cognitive phenotypes (e.g., typical older adults and amnesic

mild cognitive impairment [aMCI]) is small (Lin et al., 2017). Compared to ANS at rest, dynamic ANS changes in response to environmental demands are more closely linked to brain function but less affected by cardiovascular or neurodegeneration factors (Forte, Favieri, & Casagrande, 2019; Gianaros, Van Der Veen, & Jennings, 2004; Park, Vasey, Van Bavel, & Thayer, 2013). For example, it has been shown that increased task difficulty results in decreased ANS activity during a working memory task (Gianaros et al., 2004). When engaging in cognitive challenges, the initial decrease or suppression phase of the ANS response occurs when the frontal circuit must allocate neural resources in response to cognitive demand, thereby suffering from diminished capacity to exert control over the ANS. The subsequent increase or rebound phase represents the return of neural resources in regulating the ANS when individuals have learned and cognitive demands are no longer challenging enough to require additional neural resources. This entire process—suppression and then rebound of the ANS—in response to a cognitive challenge reflects adaptation capacity. In terms of plasticity, it has been suggested that positive plastic changes in brain and behavior are driven by a mismatch between supply and demand, wherein cognitive demand exceeds available neural resources (Lövdén et al., 2010). This mismatch arising due to a cognitive challenge appears to overlap with suppression of the ANS response; as cognitive demand is no longer challenging, the decline in the mismatch overlaps with rebound of the ANS response (see Figure 1a). Synthesizing the neurovisceral integration (Thayer & Lane, 2000) and mismatch (Lövdén et al., 2010) frameworks, we suspect that ANS responses during cognitive demand may explain individual differences in learning.

We recently completed a phase II double-blinded randomized controlled trial, comparing neurocognitive effects of a 6-week vision-based speed of processing training (VSOP) and a mental leisure activities (MLA) active control in older adults with aMCI (Lin et al., 2020).

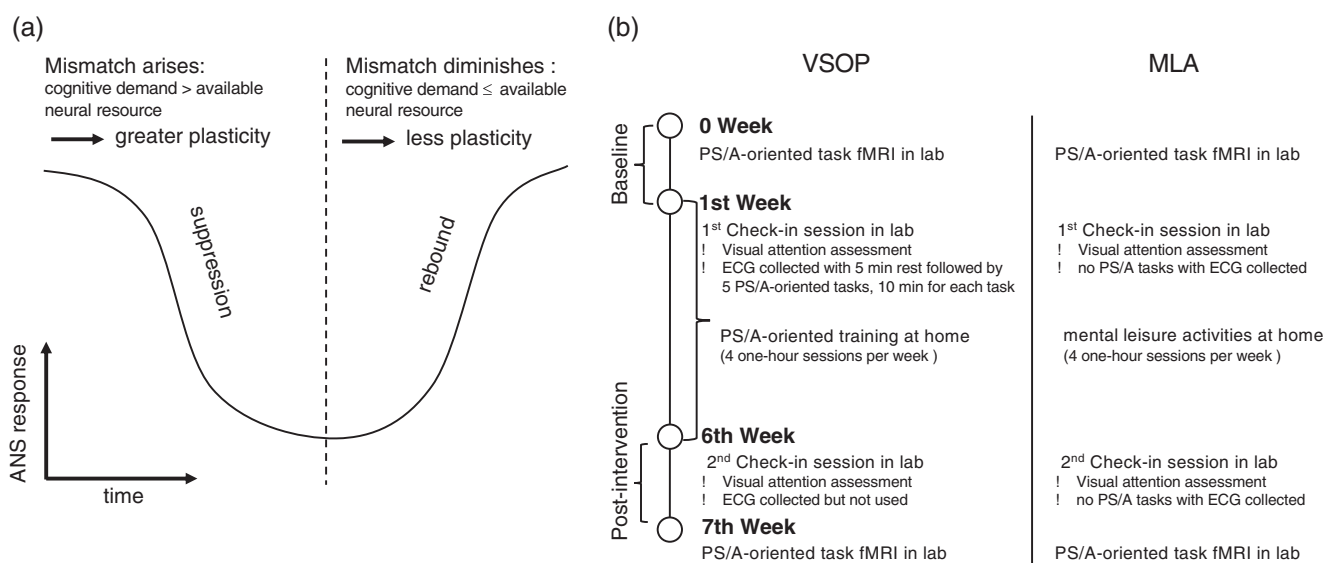


FIGURE 1 (a) A simple toy example to visualize and help understand the neurovisceral integration (Thayer & Lane, 2000) and mismatch (Lövdén et al., 2010) frameworks. (b) Schematic description of the experimental design. ANS, autonomic nervous system

TABLE 1 Participant information

	VSOP (<i>n</i> = 46)	MLA (<i>n</i> = 28)	<i>T</i> or χ^2 test, <i>df</i> , (<i>P</i>)
Age, mean (<i>SD</i>)	75.13 (7.56)	73.68 (6.92)	0.83, 72 (.41)
Years of education, mean (<i>SD</i>)	15.98 (2.29)	16.68 (2.87)	-1.16, 72 (.25)
Male, <i>n</i> (%)	27 (58.7)	13 (46.4)	1.05, 1 (.30)
Non-Hispanic White, <i>n</i> (%)	43 (93.5)	13 (46.4)	3.62, 1 (.06)
Married, <i>n</i> (%)	34 (73.9)	22 (78.6)	0.05, 1 (0.82)
MOCA, mean (<i>SD</i>)	24.24 (2.65)	20 (71.4)	-0.19, 72 (.85)
GDS, mean (<i>SD</i>)	2.30 (2.23)	1.75 (2.40)	1.00, 72 (0.32)
Single-domain aMCI, <i>n</i> (%)	18 (39.1)	15 (53.6)	1.47, 1 (0.23)
First-degree family history of AD, <i>n</i> (%)	24 (52.2)	15 (53.6)	0.01, 1 (.91)
ADSCCT, mean (<i>SD</i>)	2.74 (0.17)	2.81 (0.14)	-1.89, 72 (.06)
Taking AD medication, <i>n</i> (%)	7 (15.2)	3 (10.7)	0.30, 1 (0.59)
BMI, mean (<i>SD</i>)	26.20 (4.42)	26.86 (4.50)	-.634, 72 (0.53)
Chronic condition index, mean (<i>SD</i>)	4.46 (2.16)	4.64 (2.34)	-.349, 72, (.73)
Hypertension, <i>n</i> (%)	21 (45.7)	18 (64.3)	2.15, 1 (.14)
Diabetes, <i>n</i> (%)	7 (15.2)	1 (3.6)	2.45, 1 (.12)
Total amount of training time in hour, mean (<i>SD</i>)	18.01 (7.1)	25.30 (7.78)	-4.13, 71 (<.000)
Executive function at baseline, mean (<i>SD</i>)	-0.11 (0.54)	-0.06 (0.52)	-0.38, 72 (.70)
Episodic memory at baseline, mean (<i>SD</i>)	39.2 (13.69)	38.96 (12.22)	0.07, 72 (.94)
Visual attention at baseline, mean (<i>SD</i>)	5.87 (0.53)	5.89 (0.50)	-0.19, 70 (.85)
Visual attention after intervention, mean (<i>SD</i>)	5.52 (0.49)	5.76 (0.48)	-2.08, 72, (.04)

Note: Visual attention was measured by log-transformed Useful Field of View (lower is better). Bold values indicate $p < .05$.

Abbreviations: AD, Alzheimer's disease; ADSCCT, Alzheimer's disease signature cortical thickness (for neurodegeneration); aMCI, amnesic mild cognitive impairment; BMI, body mass index; GDS, Geriatric Depression Scale—15 items; MOCA, Montreal Cognitive Assessment (for global cognition).

VSOP trains processing speed and attention (PS/A), a cognitive domain essential to arguably all cognitive operations (Salthouse, 1996; Woutersen et al., 2017). Comparison of VSOP and MLA from baseline to immediate post-intervention showed a significant training effect on visual attention that was not practiced in the VSOP training (Table 1). The VSOP group also had significantly greater PS/A task-related activation in dorsal anterior cingulate cortex and inferior and superior frontal gyri (Figure S1A) after intervention compared to the MLA group. Furthermore, the increased activations observed in the VSOP group were associated with greater improvement in the visual attention measure (Figure S1B).

In the present study, we examined whether any segments of the ANS response to cognitive challenges can prospectively predict VSOP-induced learning and associated neuroplasticity. We monitored learning and task-based fMRI activity during PS/A related cognitive challenges before and after VSOP, and ANS flexibility at the beginning and end of the VSOP intervention period. ANS flexibility was indexed using high frequency heart rate variability (HF-HRV) extracted from electrocardiography (ECG) data. HF-HRV has been shown to reflect how the parasympathetic branch of the ANS sensitively and timely, to millisecond, responds to the changing environment (Zahn et al., 2016). We used a machine learning approach called shapelet analysis (Ye & Eamonn, 2009; Ye & Keogh, 2010) to

identify ANS responses predictive of learning. A shapelet is a time-series subsequence used as a reference predictor for an outcome of interest. In our case, a candidate shapelet was chosen from its similarity values to optimize the prediction of learning. Similarity values are distance measures (in our case, Pearson correlation) between a candidate shapelet and its best matching subsequences from time-series.

Applying this analytical approach, we identified a 2-min ANS shapelet, indexed by an initial increase in HF-HRV, in response to PS/A tasks at baseline that aligns with the rebound phase of ANS flexibility. The ANS shapelet predicted individual variability in learning, as well as the change in PS/A task-related fMRI activity after cognitive training. Specifically, participants with HF-HRV segments that were more similar to the identified ANS shapelet had poorer training outcomes of learning and neuroplasticity. The predictive capacity of the ANS shapelet was robust and generalizable across participants and learning from multiple PS/A tasks. Moreover, the predictive ability of the shapelet was not influenced by age, years of education, neurodegeneration, or total cognitive training time. In sum, we found strong evidence supporting the premise that ANS flexibility contributes independently to inter-individual differences in learning and neuroplasticity during cognitive training.

2 | METHODS

2.1 | Design

The protocol for the parent double-blinded randomized controlled trial was reported previously (Lin et al., 2020). In the current study, we focused on participants from the VSOP group to examine the relationships between ANS patterns, learning, and neuroplasticity. ANS function and learning were assessed using ECG and performance data collected at two check-in sessions, one during the first week and the other during the last week of the 6-week intervention period. We did not collect ECG and PS/A-related performance data from the MLA group at the two check-in sessions to minimize exposure to the VSOP tasks. PS/A-induced neuroplasticity was assessed using data from PS/A task-based fMRI at baseline and post-intervention in both groups. By contrasting VSOP with MLA group, we identified brain areas that showed significant intervention-induced neuroplasticity. Protocol of the current study is presented in Figure 1b.

2.2 | Participants

Eighty-four older adults with amnesic MCI (single- or multiple-domain) aged 60–90 years were recruited from University-affiliated memory, internal, and geriatric clinics. All clinics used 2011 diagnostic criteria for aMCI (Albert et al., 2011): (a) memory deficit (1–1.5 *SD* below age- and education-corrected population norms); (b) may have deficits in other cognitive domains (e.g., executive function); (c) preserved Basic Activities of Daily Life, defined as requiring occasional assistance on less than two items on the Minimum Data Set-Home Care interview; and (d) absence of dementia using NINCDS-ADRDA criteria. Other inclusion criteria included (a) if applicable, no change in dose of Alzheimer's medication (i.e., memantine or cholinesterase inhibitors) in the 3 months prior to recruitment; (b) capacity to give consent based on clinician assessment; and (c) other: age \geq 60 years, English-speaking, adequate visual acuity for testing, and community-dwelling. Exclusion criteria included (a) current enrollment in another cognitive improvement study; (b) uncontrollable major depression, or change of antipsychotic, anti-seizure med, antidepressants or anxiolytics in the past 3 months; (c) MRI contraindications (e.g., pacemaker); (d) major vascular disease: stroke, myocardial infarction, or congestive heart failure. The study was approved by the University of Rochester Research Subject Review Board. Written consent was obtained from each participant. Since cognitive assessments vary across clinics, we reassessed memory (Brief Visuospatial Memory Test (Benedict, 1997), executive function (EXAMINER, Kramer et al., 2014), and global cognition (Montreal Cognitive Assessment; Rossetti, Lacritz, Cullum, & Weiner, 2011) at baseline. Background information is presented in Table 1.

2.3 | Intervention

Participants were randomized to VSOP or MLA at a 2:1 ratio. PS/A-oriented cognitive training was administered using a commercial

package from Posit Science called BrainHQ, which included five computer games that target PS/A. All tasks share visual components, and the tasks become increasingly more difficult and require faster reaction times as training progresses. Participants respond by identifying either the type or location of an object displayed on the screen. The training dynamically adjusts the difficulty of each task in real time based on the participant's performance, ensuring that participants always operate near their optimal capacity. If participants achieve an 80% accuracy rate across all five tasks, the training program will advance to the next difficulty level. MLA intervention included online crossword, Sudoku, and solitaire. Participants were allowed to select any combination of these games during each training session. The purpose of MLA was to control for computer and online experiences and duration of training time, as well as to simulate everyday mental activities. For both groups, we provided identical online platforms, an orientation, and two in-person check-in sessions. Participants completed all subsequent training sessions at home. During the self-administration period, technical support was available by phone and email. The training period for both groups lasted 6 weeks, and participants were instructed to complete four 1-hr sessions per week.

2.4 | Check-in sessions

For VSOP group, task paradigms with fixed stimuli that targeted PS/A but differed from the PS/A-oriented training were used in the check-in sessions to evaluate reaction time-based learning scores. Each participant began with a 5-min resting period, then completed the 5 PS/A tasks (multiple object tracking [MOT]; rapid serial visual presentation [RSVP]; Search, Sweep, and useful field of view [UFOV]). Each task lasted for 10 min, using a 1-s fixation point and a 2-s inter-stimulus interval, with a response window of either 6 s (MOT, Search, and Sweep) or 10 s (RSVP and UFOV). Task order was randomized across participants and across the two sessions. Figure 2a shows examples of stimuli used in the tasks. Individual task paradigms are described in Supporting Information.

2.5 | Measures

Learning was assessed for each task separately for VSOP group using data from the two check-in sessions. Learning was calculated as the difference between the averaged reaction time of trials with correct responses in the two sessions, controlled for the first check-in session, then converted to z-scores within each task. Higher scores indicated greater reduction in reaction time and more effective learning. We excluded 7 participants who dropped out of the study during the intervention period (refer to CONSORT form, Figure S2).

ECG data were acquired with Mindware 2-Slot BioNex model and BioLab software and monitored continuously using a standard lead-II electrode configuration during the rest period and while participants completed the five PS/A tasks during the two check-in sessions. HF-HRV, an index for parasympathetic ANS activity, was preprocessed

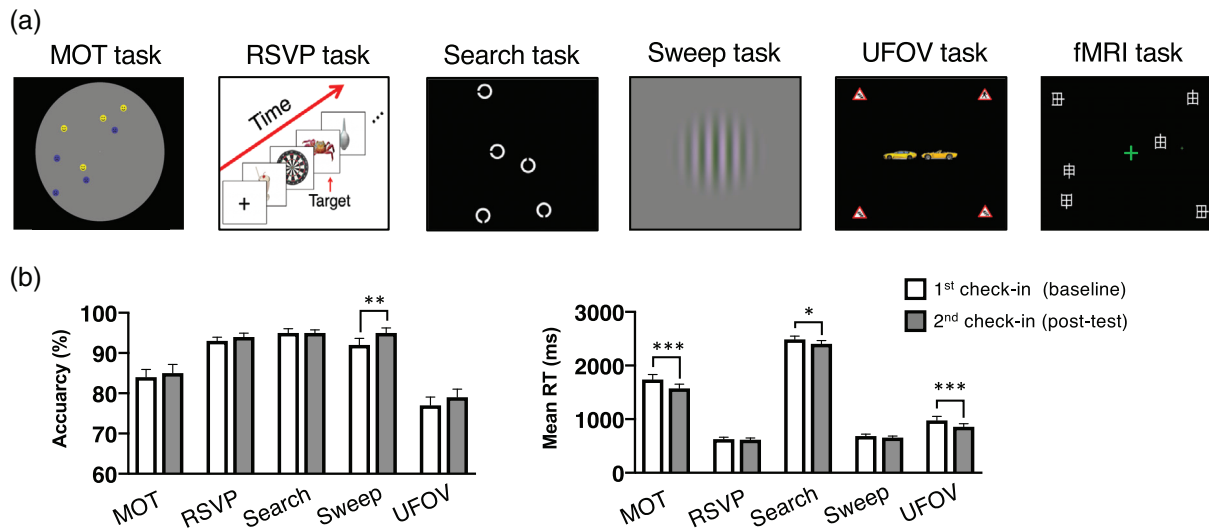


FIGURE 2 (a) Sample stimuli for check-in sessions and fMRI. (b) The accuracy and mean reaction time for the two check-in sessions and corresponding standard errors of the mean are shown. The mean reaction time was calculated for correct responses only. Black asterisks indicate statistical significance with one-tailed paired t-tests between the two sessions (* $p < .05$; ** $p < .01$; *** $p < .001$). MOT, multiple object tracking; RSVP, rapid serial visual presentation; UFOV, useful field of view

with Mindware HRV analysis software (v3.1), using methods described previously (Berntson et al., 1997). An R-R interval is the time elapsed between two successive beats on the electrocardiogram. Briefly, consecutive R-R intervals filtered at 0.12–0.40 Hz to generate HF-HRV and natural log transformed. We extracted 15-s segments and removed ectopic beats and artifacts by consistent visual inspection between two raters. Null values from motion and arrhythmic artifacts in the remaining data were excluded by dividing the number of null-absent segments by the total number of segments to obtain the percentage of usable data for each participant. An 80% threshold was applied to determine valid rest and task data. Average HF-HRV was calculated for surviving resting HF-HRV data (44 observations for 44 participants). For task data, participants were included as long as they had valid data for at least one task. After removing artifacts, 41 participants had valid data for all 5 tasks. For the remaining participants, 3 had 4 tasks, 1 had 3 tasks, 1 had 2 tasks. None had valid data for only one task. Three participants without valid data for any tasks were excluded. Surviving task data (222 observations for 46 participants in total) was analyzed with the shapelet analysis approach described in the methods section. Of note, ECG data from the second check-in session was not included here because of the potential top-down effect of cognitive training on the ANS response, which may complicate the interpretation of post-training ANS signals.

MRI data were collected at University of Rochester Center for Advanced Brain Imaging and Neurophysiology (UR CABIN), using a dedicated research 3T Siemens TrioTim scanner (Erlangen, Germany), equipped with a 32-channel head coil. **Structural MRI:** Each fMRI session began with a localizer scan, followed by an MPRAGE scan (TR/TE = 2,530 ms/3.44 ms, TI = 1,100 ms, FA = 7, 256 × 256 matrix, 1 mm³ isotropic resolution, 1 mm slice thickness, 192 slices) to acquire high-resolution structural-weighted anatomical images. **Task-related fMRI:** Task-related BOLD data were collected using a gradient

EPI sequence (TR/TE = 2,500 ms/30 ms, FA = 90, 64 × 64 matrix, 4 mm³ in-plane resolution, 4 mm slice thickness, 37 axial slices). A 5-min block-design visual search task (Figure 2a) was used to assess changes in brain activation. The stimuli were presented in 5 blocks, each of which consisted of 6 trials, for a total duration of 42 s; blocks were alternated with fixation periods of 20 s. Within each trial, a central fixation cross was presented for 500 ms, followed by a 5,500 ms presentation of the search pattern. An interval of 1,000 ms was inserted between trials. Participants were instructed to search for the target symbol, “申” (present for 50% of trials), displayed among six distractors in different orientations (e.g., “由”, “甲”). Participants responded by pressing one of two response buttons to indicate whether the target was present or absent. For the VSOP group, participants with two complete scan sessions (before and after intervention) and valid ECG data from the first check-in session were included in the image analysis ($n = 35$).

Background information collected at baseline included demographic information and health history. Cortical thickness signature for Alzheimer's disease-associated neurodegeneration was calculated using structural MRI data in several posterior brain regions, including bilateral inferior and middle temporal lobes, entorhinal cortex, and fusiform gyrus, which have been shown to be particularly vulnerable to Alzheimer's disease pathology (Jack Jr. et al., 2015). Details can be found in Table 1.

Visual attention was measured using Useful Field of View (UFOV), a three-task computer test that assesses processing speed, sustained attention, and divided attention based on reaction time. A composite score with natural log transformation was used, with higher scores indicating slower reaction time and poorer performance. Of note, UFOV used here is different from the aforementioned UFOV used in the ECG collection which is a simplified version. The tasks in UFOV were conceptually identical to VSOP training but in different formats.

We found VSOP group showed faster reaction times than MLA group after intervention ($t = -2.08, p = .04$, Table 1).

2.6 | Data analysis

Shapelet analysis: We used a machine learning approach called shapelet analysis (Ye & Eamonn, 2009; Ye & Keogh, 2010) to identify ANS responses that are predictive of learning. Traditional linear analyses that use summary scores (e.g., means) discard information about the shape of a time series, while shapelet analysis preserves the local shape of the time series. Furthermore, compared to nonlinear methods, such as approximate entropy, that are heavily dependent on the recording length, the shapelet-based method is capable of capturing temporally ordered features at both local (small window size) and global (large window size) scales, allowing for more flexible and robust detection of subtle, dynamic changes in data. Together these characteristics support the use of shapelet analysis to analyze the time course of ECG.

There are six steps involved in determining whether any baseline HF-HRV shapelets can predict learning after intervention (Figure 2):

1. *Candidate extraction:* We first separated data into training and testing sets. For the training set, we extracted all possible subsequences using a sliding window with a varied window size ($W = 3, 4, 5, \dots, L$) and fixed step size ($s = 1$). Total number of candidates was calculated as $N \times \sum_{W=3}^L (L - W + 1)$, N : number of training sample, L : length of a time series, which was 40 segments (15 s/segment for total 10 min); W : sliding window size.

2. *Subsequence transformation:* Using the candidates, HF-HRV data was transformed into a similarity matrix and used as features. For each candidate shapelet C and a given time series T , we obtained the similarity in the following way:

$$\text{maxPearsonSimilarity}(C, T) = \max_{i=1, 2, \dots, L-W+1} \frac{\text{cov}(C, T_{i:i+W-1})}{\sigma_C \sigma_{T_{i:i+W-1}}}$$

where W is the length of the candidate C , $T_{i:i+W-1}$ are the observations of T at $i, i+1, i+2, \dots, i+W-1$ time point, σ_C are the standard deviation of C , $\sigma_{T_{i:i+W-1}}$ are the standard deviation of $T_{i:i+W-1}$, and $\text{cov}(C, T_{i:i+W-1})$ is the covariance of C and $T_{i:i+W-1}$.

In other words, the similarity to a candidate was the similarity between a candidate and its best matching subsequence of a time series.

3. *Shapelet selection:* For the training set, candidates were ranked based on the absolute value of the correlation between the features (similarities to the candidates) and the learning scores. The highest ranked candidate was selected for further use, and the remaining candidates were removed.

4. *Model learning:* For training set, we used linear regression to model the relationship between similarities to the selected shapelet and learning scores:

$$\min_{a, b} \|Y - (aX + b)\|,$$

where X contains the selected features (similarities to the selected shapelet), Y contains the learning scores, and a, b are the regression coefficients.

5. *Label prediction:* We applied the trained model to predict the learning score of the testing set. The predictor was the similarity to the selected shapelet calculated as described in Step 3.

6. *Evaluation:* We evaluated the results by examining the correlation between the predicted and actual outcomes of testing data. To evaluate the significance of our result, we performed permutation test shuffling the labels among the samples. The permutation p -value was reported as (number of permutation $R > \text{true } R$)/number of permutations.

We first performed leave-one-participant-out cross-validation (see Figure 3a). The model was trained on $n - 1$ participants and tested on the participant who was excluded from the iteration. This process was repeated for all 46 participants. We evaluated the results from the testing data across all iterations. We then performed cross-task validation to examine whether there was a task-independent HF-HRV shapelet (see Figure 5a). We trained the model on 4 of the 5 tasks and tested on the excluded task. This process was repeated five times, wherein each training iteration reserved one task for testing. Results from each task (iteration) were evaluated separately.

Additionally, we repeated leave-one-participant-out cross-validation with the candidate shapelet identified from the first round of cross-validation using fixed segment lengths to examine how the length of the shapelet might influence the prediction results. In other words, we performed shapelet analysis separately for each possible segment length (i.e., 3, 4, ..., 40 segments). The candidate shapelet selected in each iteration was the one whose predictive value was highest for the learning scores associated with the given segment length.

Image data preprocessing and analysis: fMRI data were analyzed with FEAT FSL Version 6.0.0 (www.fmrib.ox.ac.uk/fsl) (Smith et al., 2004; Woolrich et al., 2009) and in-house Matlab scripts. Preprocessing of the functional data was performed in the following order: slice time correction (sinc interpolation), motion correction to the middle volume, smoothing with a nonlinear algorithm using a 5 mm kernel, and high-pass temporal filtering with $\sigma = 100$ s. For each participant, functional data were registered to high-resolution brain-extracted anatomical images in native space. Functional and anatomical volumes were transformed into standardized MNI space.

For task fMRI, a general linear model was used to fit beta estimates to the task condition and convolved with a standard Double-Gamma hemodynamic response function. The six motion parameters were added to the model as regressors of no interest to address variance attributable to head movement. Individual participant data were analyzed to test for the contrast of "task > fixation." These contrast maps were then used for a subsequent group-by-time analysis. To examine the intervention-induced neuroplasticity effect, we compared VSOP with MLA group. We calculated the interaction between Group (i.e., VSOP vs. MLA) and Visit Time (Post-intervention vs. Baseline) using FLAME (FMRIB's Local Analysis of Mixed Effects).

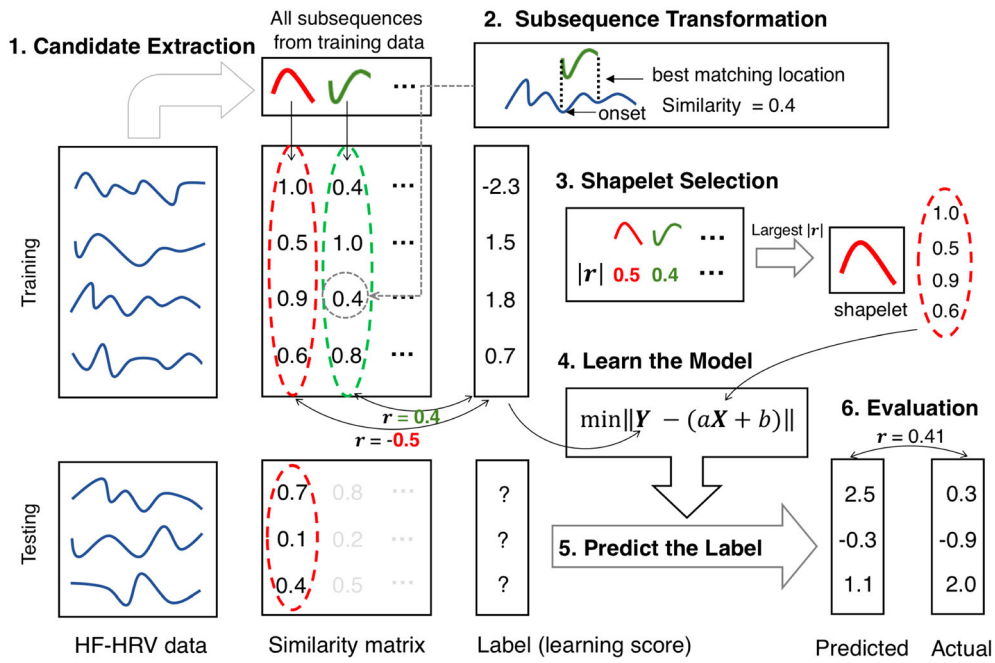


FIGURE 3 An illustration of the shapelet analysis with synthetic data. First, from all time series in training data, subsequences of a specific length (3–40 segments, 15 s/segment) were extracted to be candidates using a sliding window approach. Second, we generated features from time series using the similarity between a candidate and its best matching subsequence of a time series. Third, we selected the shapelet most associated with the learning score. Fourth, we used linear regression to model the relationship between similarities of the selected shapelet and learning scores. Fifth, we applied the trained model to predict the learning score of the testing set. Lastly, we evaluated the results by examining the correlation between the predicted and actual outcomes of testing data. To evaluate the significance of the test results, we did a permutation test by shuffling the labels among the samples. The permutation p value was reported as (number of permutation $R >$ true R)/number of permutations. This procedure was used in both cross-participant and cross-task analyses. HF-HRV, high frequency heart rate variability. HF-HRV data were collected from the first check-in session. Learning scores were calculated as the difference between the averaged reaction time of correct-response trials for each PS/A task in the two check-in sessions, controlled for the averaged reaction time from the first check-in session, and converted to z-scores within each task

The resulting whole brain Z (Gaussianised T/F) statistic image was thresholded with $Z > 1.7$ and a corrected cluster significance threshold of $p < .05$ based on Gaussian random field theory.

Next, we tested the relationship between the ANS responses and the intervention-induced neuroplasticity for VSOP group. We extracted percent signal change within 9 mm radius spheres around the peak activation derived from the whole brain interaction analysis and calculated the change of activation from baseline to post-intervention for each individual. ANS responses were assessed by the averaged similarity to Shapelet A across the five tasks in the first check-in session for each participant. Pearson correlations were performed between ANS responses and change in activation.

Other data analysis was conducted using SPSS 24.0. We compared behavioral performance between the two check-in sessions using paired t -tests. We did post hoc analyses based on the shapelet identified in the cross-participant analysis, using linear mixed models with participant as a random effect.

First, we examined the relationship between shapelet similarity and learning based on the onset time of the selected shapelet, controlling for the main effects of onset time and similarity of the shapelet and type of task ($y_{\text{Learning}} = \beta_0 + \beta_1 \text{ Task} + \beta_2 \text{ Similarity to}$

Shapelet + $\beta_3 \text{ Onset Time} + \beta_4 \text{ Similarity to Shapelet} \times \text{Onset Time} + \epsilon$). The onset of the selected shapelet was defined as the beginning of the best match location to the selected shapelet in a time series data. Any significant interaction effect between “Similarity to Shapelet” and “Onset Time” suggests that the predictive value of the shapelet is modulated by the time at which the shapelet appears.

Next, we examined the effect of covariates (age, education, neurodegeneration, total training time, or resting HF-HRV) on the similarity to the selected ANS shapelet ($y_{\text{Similarity to Shapelet}} = \beta_0 + \beta_1 \text{ Task} + \beta_2 \text{ Covariate} + \epsilon$), controlling for type of task. Resting HF-HRV was assessed by averaged HF-HRV during the rest period. We also tested the prediction of task HF-HRV on learning while controlling for covariate and type of task ($y_{\text{Learning}} = \beta_0 + \beta_1 \text{ Task} + \beta_2 \text{ Covariate} + \beta_3 \text{ Similarity to Shapelet} + \epsilon$).

Additionally, we tested the prediction of the similarity to the selected ANS shapelet on intervention-induced neuroplasticity while controlling for covariates. We computed partial Pearson correlations between averaged similarity to the selected shapelet across the five tasks and the change of activation from baseline to post-intervention, controlling for age, education, neurodegeneration, and total training time.

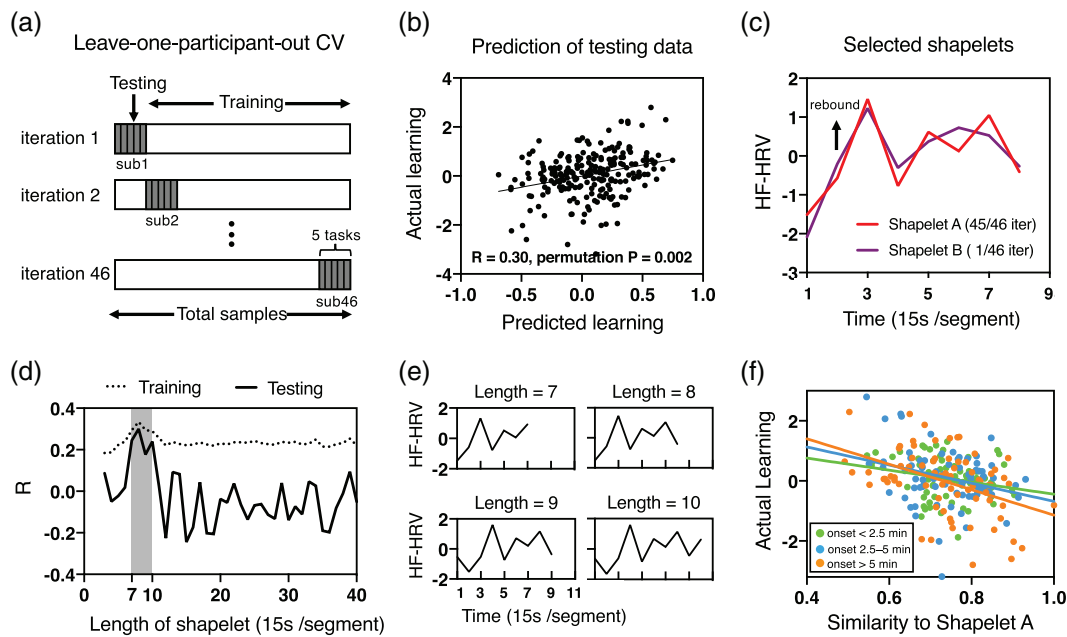


FIGURE 4 (a) Schematic description of the cross-participant validation. (b) Scatterplot of the predicted learning score using HF-HRV at baseline. The x-axis is the predicted learning score and the y-axis is the observed learning score. (c) Selected shapelets from the training. The HF-HRV value is plotted on the y-axis, and time, represented by segments, is plotted on the x-axis. One segment represents 15 s. Shapelet A (in red) was identified in 45 out of 46 iterations and Shapelet B (in purple) was identified once. The two shapelets were highly similar. (d) Prediction of learning with fixed segment lengths of the shapelets. The y-axis is the linear correlation between the predicted learning score and the observed learning score. The solid black line is the prediction of from testing set, and the dotted black line represents the prediction from the training set. Significant predictions from testing data were achieved with fixed lengths of 7, 8, 9, and 10 segments. (e) The shapelets selected with the highest frequency for lengths with successful predictions. (f) Scatterplot of the similarity to Shapelet A and the learning score for participants with different onset times. We grouped participants into terciles based on the onset time of Shapelet A: Early (1–33.3%, <2.5 min; green), middle (33.3–66.6%, 2.5–5 min; blue) and late (66.6–100%, >5 min; orange)

3 | RESULTS

3.1 | Behavioral results related to learning after intervention

After the 6-week training there was a significant improvement in accuracy for Sweep ($t[45] = -3.09, p = .002$) and a reduction in reaction times for MOT ($t[45] = -3.31, p < .001$), Search ($t[45] = 1.75, p = .04$), and UFOV tasks ($t[45] = 3.305, p = .001$; see Figure 1c). Learning scores were calculated as the difference between the averaged reaction time of correct-response trials for each PS/A task in the two check-in sessions, controlled for the averaged reaction time from the first check-in session, and converted to z-scores within each task. Individual task paradigms are described in Supporting Information.

3.2 | Identify baseline ANS shapelets that are predictive of learning after intervention

Cross-participant prediction and validation: We first examined whether HF-HRV—a gold standard index for vagal control of ANS flexibility—in response to PS/A-oriented tasks at baseline (i.e., the first check-in session) could predict learning after the 6-week training across

participants. We utilized a shapelet analysis (Figure 2) with leave-one-participant-out cross-validation, as shown in Figure 4a. In each leave-one-participant-out iteration, we retained one participant for testing and used the remaining participants for training. This was repeated for all 46 participants, thus resulting in 46 iterations. We searched for an HF-HRV shapelet for which the similarity could best predict learning during training and evaluated the result on testing data across all iterations. We found baseline HF-HRV significantly predicted learning on the testing set ($R = 0.30, \text{permutation } p = .002$; Figure 4b). Two shapelets (Shapelet A and Shapelet B, Figure 4c), both featuring a length of 8 segments (15 s/segment for a total of minutes) and an initial rise in HF-HRV, were identified from the training set (Figure 4c). The former shapelet was identified in 45/46 iterations and the latter shapelet in 1/46 iterations. The two shapelets were highly correlated ($R = 0.90, p = .003$). Furthermore, the similarity between Shapelet A/B was negatively correlated with the learning score ($R = -0.34, p < .001$ for Shapelet A; $R = -0.28, p < .001$ for Shapelet B), suggesting that a participants were more likely to benefit from the 6-week training if their best matching subsequence over the 10-min task was more *dis-similar* to Shapelet A/B at baseline.

To determine whether the shapelet length might influence the prediction, we repeated our analysis with different shapelet segment lengths. Statistically significant prediction results from the testing set

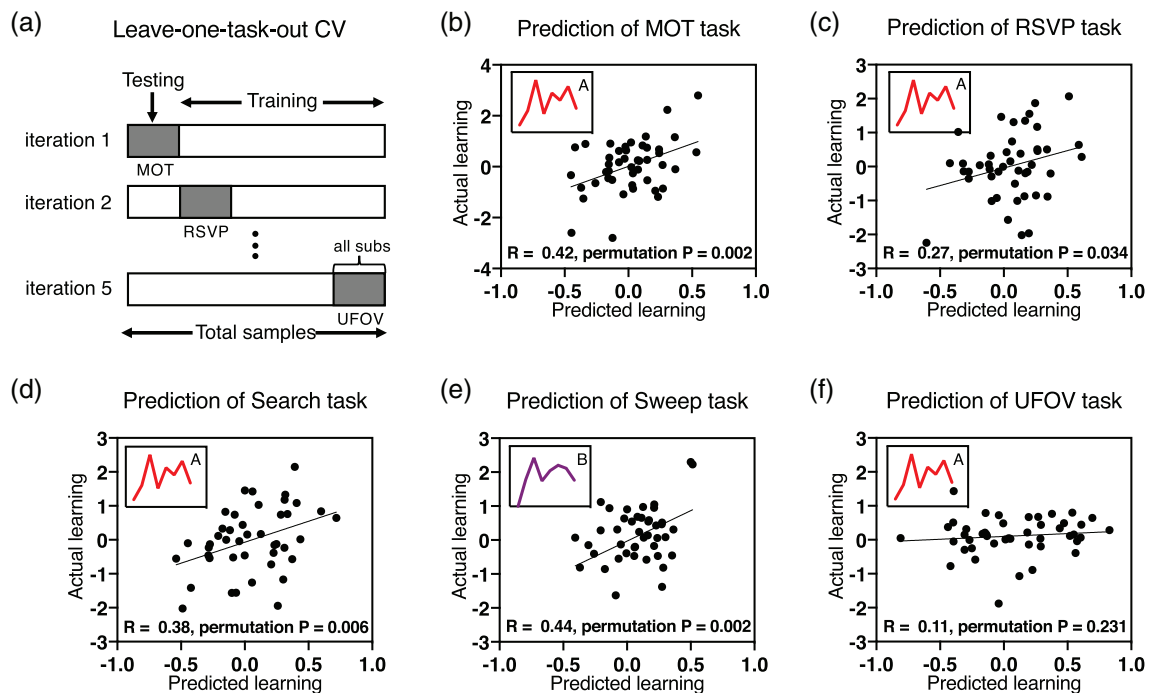


FIGURE 5 (a) Schematic description of the cross-task validation. (b–f) Scatterplot of the learning score prediction using HF-HRV at baseline for each task, separately. The x-axis is the predicted learning score and the y-axis is the observed learning score. The shapelets selected with the highest frequency are plotted in the upper left corner

were achieved with a length of 7–10 segments (1.75 to 2.5 min; $R = 0.25$, permutation $p = .026$ for length of 7; $R = .30$, permutation $p = .002$ for length of 8; $R = .18$, permutation $p = .05$ for length of 9; $R = .24$, permutation $p = .031$ for length of 10). The model achieved highest performance in both training and test sets using an 8-segment length (2 min) (Figure 4d). We also discovered that the shapelets with lengths of 7 to 10 segments all featured an initial rise in HF-HRV (Figure 4e). Therefore, our method was robust to the selection of shapelet length.

Cross-task prediction and validation: We were also interested in evaluating whether there were any *generic*, or task-independent, baseline HF-HRV shapelets. Here, we conducted a shapelet analysis (Figure 2) with leave-one-task-out cross-validation (see Figure 5a for the cartoon illustration of our data split). In each leave-one-task-out iteration, we retained one task for testing and used the remaining tasks for training. This was repeated for all five tasks, thus resulting in five iterations. The results are displayed in Figure 5b–f. Baseline HF-HRV in response to task significantly predicted learning in 4 out of the 5 PS/A-oriented tasks (MOT: $R = 0.42$, permutation $p = .002$; RSVP: $R = 0.27$, permutation $p = .034$; Search: $R = 0.38$, permutation $p = .006$; Sweep: $R = 0.44$, permutation $p = .002$; UFOV: $R = 0.11$, permutation $p = .231$). Similar to the cross-participant analysis, Shapelets A and B were revealed again in the cross-task analysis. The former shapelet was identified in 4 out of 5 tasks and the latter shapelet in 1 task.

In the following analyses, we focused only on Shapelet A (i.e., the shapelet with the best prediction results out of all significant shapelets on both the training and test sets in the cross-participant analysis).

For each participant and each task, the degree of similarity between each HF-HRV task segment and Shapelet A was calculated using a sliding window approach with a 2-min window size. The task segment that shared the highest degree of similarity with Shapelet A was considered representative of a given task for a given participant. Then the averaged similarity with Shapelet A across 5 tasks for each participant was used in the subsequent analysis.

3.3 | Relationships between similarity of the selected ANS shapelet and neuroplasticity after cognitive training

For the PS/A fMRI task, we first calculated intervention-induced neuroplasticity based on the interaction between Group (VSOP vs. MLA) and Visit Time (Post-intervention vs. Baseline). We revealed three ROIs—dorsal anterior cingulate cortex (dACC), superior frontal gyrus (SFG), and inferior frontal gyrus (IFG)—where we found that, relative to MLA, VSOP group had significantly greater increases in activation from baseline to post-intervention (Figure 6a). Next, we tested the relationship between the similarity to the selected ANS shapelet and the intervention-induced neuroplasticity for the VSOP group. The intervention-induced neuroplasticity was assessed by the increase of activation from baseline to post-intervention in the three ROIs. The similarity to the selected ANS shapelet significantly predicted intervention-induced neuroplasticity in dACC ($R = -0.34$, $p = .022$) and SFG ($R = -0.31$, $p = .035$) (see Figure 6b), but not in IFG ($R = 0.22$, $p = .10$).

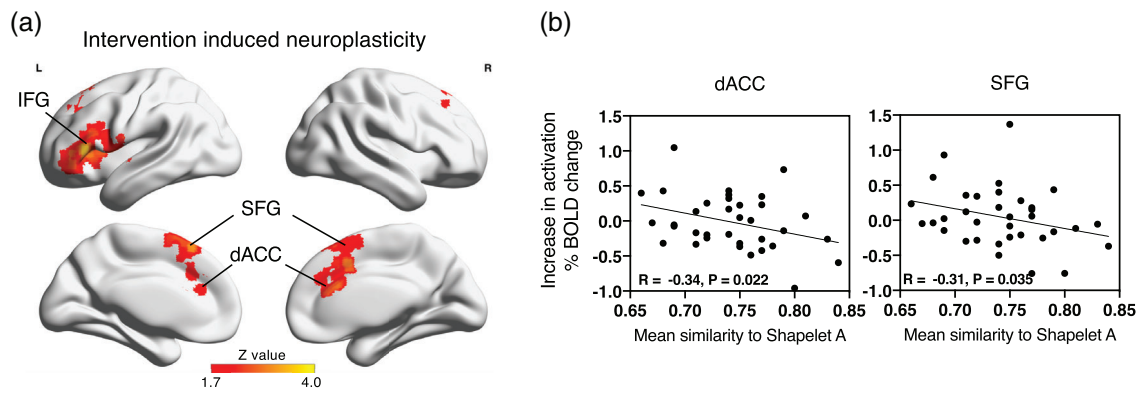


FIGURE 6 (a) Intervention-induced neuroplasticity measured with task-based fMRI. Intervention-induced neuroplasticity was calculated by the interaction between Group (VSOP vs. MLA) and Visit Time (Post-intervention vs. Baseline). Compared to MLA group, a significantly greater increase from baseline to post-intervention was found for VSOP group in dACC (cluster size: 388 voxels, peak z-value = 2.91, MNI coordinate: 2 24 24), SFG (cluster size: 999 voxels, peak z-value = 3.07, MNI coordinate: -8 24 54) and left IFG (cluster size: 1119 voxels, peak z-value = 3.57, MNI coordinate: -52 28 8). (b) ANS responses predict intervention-induced neuroplasticity in dACC and SFG. The y-axis in the scatter plots is the change in activation from baseline to post-intervention in dACC and SFG. The x-axis is the averaged similarity to Shapelet A across five tasks for each individual at baseline. Mean similarity to Shapelet A negatively correlated with increased activation in dACC and SFG. dACC, dorsal anterior cingulate cortex; IFG, inferior frontal gyrus; SFG, superior frontal gyrus

3.4 | Additional considerations for the relationship between the selected ANS shapelet and learning/neuroplasticity

The correlational strength between similarity to the selected ANS shapelet and learning was based on the onset time of the shapelet: The average onset of Shapelet A across participants and tasks was 3.9 ± 2.2 min. We calculated the interaction effect of onset time of a HF-HRV segment and its degree of similarity to Shapelet A on learning across all tasks, controlling for the main effects of onset time, shapelet similarity, and task type. The interaction effect was significant ($B = 0.15$, $SE = 0.08$, $t = 2.01$, $p = .046$). Figure 4f shows this relationship, which suggests that the predictive value of the shapelet for learning was stronger when the onset of the shapelet occurred later in the task.

Age, education, neurodegeneration, total cognitive training time, and resting HF-HRV did not influence the relationship between the similarity to the selected ANS shapelet and learning: We examined the effects of age, years of education, neurodegeneration (Jack Jr. et al., 2015), total training time, and resting HF-HRV on task HF-HRV. Resting HF-HRV was assessed by averaging HF-HRV during a 5-min rest period. No significant effect on the similarity to the selected ANS shapelet was found from age ($B = 0.0005$, $SE = .0009$, $t = 0.52$, $p = .61$), education ($B = 0.0035$, $SE = 0.003$, $t = 1.22$, $p = .23$), neurodegeneration ($B = 0.017$, $SE = 0.041$, $t = 0.40$, $p = .69$), total training time ($B = -0.000003$, $SE = 0.00002$, $t = -0.24$, $p = .81$), or resting HF-HRV ($B = 0.0034$, $SE = 0.003$, $t = 1.03$, $p = .30$), controlling for the type of task.

Furthermore, when controlling for resting HF-HRV and type of task, prediction of the similarity to the selected ANS shapelet for learning remained significant ($B = -2.32$, $SE = 0.53$, $t = -4.40$, $p < .001$). When controlling for resting HF-HRV and type of task, in

addition to age, education, neurodegeneration, and total training time, task HF-HRV still predicted learning ($B = -2.60$, $SE = 0.59$, $t = -4.36$, $p < .001$).

Additionally, we tested whether resting HF-HRV could predict learning. No significant predictions were found for any tasks (MOT: $R = -0.13$, $p = .42$; RSVP: $R = -.07$, $p = .64$; Search: $R = -0.10$, $p = .54$; Sweep: $R = -.08$, $p = .59$; UFOV: $R = -.08$, $p = .60$).

Age, education, neurodegeneration, and total cognitive training time did not influence the relationship between the similarity to the selected ANS shapelet and neuroplasticity: When controlling for age, education, neurodegeneration, and total training time, the similarity to the selected ANS shapelet still predicted *neuroplasticity* in dACC (partial correlation $R = -0.39$, $p = .015$) and SFG (partial correlation $R = -0.45$, $p = .006$), but not in IFG (partial correlation $R = 0.16$, $p = .203$).

4 | DISCUSSION

Applying both cross-participant and cross-task analyses, we identified a robust ANS-based shapelet (2 min in length, characterized by an initial rise of HF-HRV), whose similarity predicted learning across individuals and multiple PS/A tasks after a 6-week cognitive training paradigm in a group of older adults with aMCI. Furthermore, the similarity to the revealed ANS shapelet significantly predicted cognitive training-induced neuroplasticity, indexed by increased activation in dorsal (i.e., dACC and SFG) but not ventral (i.e., IFG) PFC from baseline to post-intervention. Across outcome measures of learning and associated neuroplasticity, individuals with an ANS segment more similar to the identified shapelet had poorer outcomes. The average onset time of the ANS shapelet was at 3.9 min during a 10-min PS/A task, with stronger predictive value for learning when the shapelet

occurred later during the task. Individual characteristics (e.g., education, neurodegeneration, age, total cognitive training time) did not influence the predictive ability of the ANS shapelet.

Although better overall ANS function has been correlated to higher cognitive function previously (Byrd, Reuther, McNamara, DeLuca, & Berg, 2014; Duschek, Muckenthaler, Werner, & del Paso, 2009), our finding is among the first to empirically support the theory of adaptation capacity to environmental demands and neuroplasticity. We discovered a meaningful segment of the ANS response related to cognitive challenges observed prior to cognitive training that predicted learning and associated neuroplasticity more than one month later. Previous studies have suggested that enhanced vagal tone, reflected by greater activation of the parasympathetic branch of the ANS, leads to improvement in cognitive processes by releasing neurohormones, particularly noradrenalin, that are related to learning and memory (Groves & Brown, 2005). Furthermore, the locus coeruleus, a nucleus in the brainstem, is the primary region containing noradrenalin and directly receives signals from and projects to the ACC (Joshi, Li, Kalwani, & Gold, 2016). Additionally, activation in dorsal PFC (e.g., dACC and SFG found here) is robustly linked to HF-HRV reactivity in response to acute cognitive stimuli across adulthood, whereas activation in ventral PFC (e.g., IFG found here) is more responsive to HF-HRV reactivity in response to emotional stimuli (Thayer, Ahs, Fredrikson, Sollers 3rd, & Wager, 2012). Activation of these dorsal PFC sub regions, therefore, may facilitate learning during PS/A tasks. Together, this evidence may explain the observed causal relationship between the HF-HRV shapelet, change in PFC, and learning.

The timing of the rise in HF-HRV, identified as a marker of learning, is consistent with the notion that neural resources will shift dynamically with changes in cognitive demand. We found that the average onset of the HF-HRV shapelet across tasks occurred approximately at the fourth minute, with the relationship between the HF-HRV shapelet and learning strengthening increasingly with a later onset. As noted previously, we found in prior work that HF-HRV during cognitive demand initially declined and then rebounded (Lin, Heffner, Ren, & Tadin, 2017). The rebound occurs when a cognitive task is no longer challenging enough to require substantial neural resources. If the rebound occurs prematurely—an indication of insufficient task difficulty or a decline in the brain-behavior mismatch—then positive plasticity can be limited, regardless of the amount of cognitive training provided. The HF-HRV shapelet may therefore indicate how rapidly individuals adapt to cognitive challenges and estimate the magnitude of adaptive brain changes individuals would experience that would benefit their learning.

There are a number of implications for adopting the discovered HF-HRV shapelet in the development of an individualized cognitive training program. Performance in existing cognitive training paradigms is often skewed by unmodifiable factors, such as education and premorbid IQ, and inflation from a large proportion of correct answers that are actually “guessing trials,” both of which can interfere with neuroplasticity. The discovered ANS pattern may be a potential biomarker for this cognitive training “mismatch”, given its predictive value for learning and neuroplasticity.

Limitations should be acknowledged. First, in cross-task analysis, prediction of the ANS shapelet was generalized to PS/A tasks, excluding UFOV. The objective of UFOV is to identify a center target while simultaneously locating a peripheral target, which can be particularly difficult, as evidenced by the lowest averaged accuracy (<80%) among all PS/A tasks. We suspect that a task duration of 10 min might be too short to detect any rebound, given the challenging difficulty level of the task. To further validate the predictive value of the revealed ANS shapelet for UFOV, a longer task may be required. Second, although we utilized multiple cognitive tasks, they all targeted PS/A. According to a recent meta-analysis, attentional control in learning is most likely related directly to ANS regulatory capacity (Zahn et al., 2016), which served as justification for testing the current phenomenon in the PS/A tasks. However, the current phenomenon needs to be further validated in other types of learning. Given the evidence for age-associated dedifferentiation of neural networks in support of different types of learning, as well as the reallocation of neural resources associated with learning to frontal regions (Dennis & Cabeza, 2011), we expect the current model to be applicable to other learning types. Additionally, although the discovered ANS shapelet is not susceptible to cortical atrophy-associated neurodegeneration, its potential susceptibility to other types of neuropathology related to aging or neurodegeneration (e.g., dopamine deficiency, amyloid or tau deposition) remains unclear and should be further examined. Finally, given the interaction between the sympathetic and parasympathetic branches of the ANS in response to environmental demands, the role of the sympathetic branch in learning needs to be examined to determine whether the predictive value of the identified ANS shapelet can be further strengthened.

By synthesizing two theories on mismatch's role in neuroplasticity and neurovisceral integration of ANS and brain, our findings are among the first empirical evidence to confirm that adaptation capacity, indexed by ANS flexibility, predicts individual differences in learning and associated neuroplasticity beyond individual characteristics.

ACKNOWLEDGEMENT

The study was supported by NIH R01 NR015452 to Feng Vankee Lin.

CONFLICT OF INTEREST

The authors declare no potential conflict of interest.

DATA AVAILABILITY STATEMENT

PHI de-identified behavioral and imaging data will be available via IRB approval.

ORCID

Quanjing Chen  <https://orcid.org/0000-0003-4630-6817>

Brian Rooks  <https://orcid.org/0000-0003-4161-1724>

REFERENCES

- Albert, M. S., DeKosky, S. T., Dickson, D., Dubois, B., Feldman, H. F., Fox, N. C., ... Snyder, P. J. (2011). The diagnosis of mild cognitive impairment due to Alzheimer's disease: Recommendations from the

- National Institute on Aging-Alzheimer's association workgroups on diagnostic guidelines for Alzheimer's disease. *Alzheimers Dement*, 7, 270–279.
- Berntson, G. G., Thomas Bigger, Jr, J., Eckberg, D. L., Grossman, P., Kaufmann, P. G., Malik, M., ... Van der Molen, M. W. (1997). Heart rate variability: Origins, methods, and interpretive caveats. *Psychophysiology*, 34(6), 623–648.
- Benedict, R. H. B. (1997). *Brief Visuospatial Memory Test-Revised professional manual*. Odessa, FL: Psychological Assessment Resources, Inc.
- Byrd, D. L., Reuther, E. T., McNamara, J. P., DeLuca, T. L., & Berg, W. K. (2014). Age differences in high frequency phasic heart rate variability and performance response to increased executive function load in three executive function tasks. *Frontiers in Psychology*, 5, 1470.
- Dennis, N. A., & Cabeza, R. (2011). Age-related dedifferentiation of learning systems: An fMRI study of implicit and explicit learning. *Neurobiology of Aging*, 32, 2318.e17–2318.e30.
- Duschek, S., Muckenthaler, M., Werner, N., & del Paso, G. A. (2009). Relationships between features of autonomic cardiovascular control and cognitive performance. *Biological Psychology*, 81, 110–117.
- Forté, G., Favieri, F., & Casagrande, M. (2019). Heart rate variability and cognitive function: A systematic review. *Frontiers in Neuroscience*, 13, 710.
- Gianaros, P. J., Van Der Veen, F. M., & Jennings, J. R. (2004). Regional cerebral blood flow correlates with heart period and high-frequency heart period variability during working-memory tasks: Implications for the cortical and subcortical regulation of cardiac autonomic activity. *Psychophysiology*, 41, 521–530.
- Groves, D. A., & Brown, V. J. (2005). Vagal nerve stimulation: A review of its applications and potential mechanisms that mediate its clinical effects. *Neuroscience and Biobehavioral Reviews*, 29, 493–500.
- Jack, C. R., Jr., Wiste, H. J., Weigand, S. D., Knopman, D. S., Mielke, M. M., Vemuri, P., ... Petersen, R. C. (2015). Different definitions of neurodegeneration produce similar amyloid/neurodegeneration biomarker group findings. *Brain*, 138, 3747–3759.
- Joshi, S., Li, Y., Kalwani, R. M., & Gold, J. I. (2016). Relationships between pupil diameter and neuronal activity in the Locus Coeruleus, Colliculi, and Cingulate cortex. *Neuron*, 89, 221–234.
- Kramer, J. H., Mungas, D., Possin, K. L., Rankin, K. P., Boxer, A. L., Rosen, H. J., & Widmeyer, M. (2014). NIH EXAMINER: conceptualization and development of an executive function battery. *Journal of the international neuropsychological society*, 20(1), 11–19.
- Lampit, A., Hallock, H., & Valenzuela, M. (2014). Computerized cognitive training in cognitively healthy older adults: A systematic review and meta-analysis of effect modifiers. *PLoS Medicine*, 11, e1001756.
- Lin, F., Heffner, K. L., Ren, P., & Tadin, D. (2017). A role of the parasympathetic nervous system in cognitive training. *Current Alzheimer Research*, 14, 784–789.
- Lin, F., Ren, P., Wang, X., Anthony, M., Tadin, D., & Heffner, K. L. (2017). Cortical thickness is associated with altered autonomic function in cognitively impaired and non-impaired older adults. *The Journal of Physiology*, 595, 6969–6978.
- Lin, F. V., Tao, Y., Chen, Q., Anthony, M., Zhang, Z., Tadin, D., & Heffner, K. L. (2020). Processing speed and attention training modifies autonomic flexibility: A mechanistic intervention study. *NeuroImage*, 213, 116730.
- Lövdén, M., Backman, L., Lindenberger, U., Schaefel, S., & Schmiedek, F. (2010). A theoretical framework for the study of adult cognitive plasticity. *Psychological Bulletin*, 136, 659–676.
- Park, G., Vasey, M. W., Van Bavel, J. J., & Thayer, J. F. (2013). Cardiac vagal tone is correlated with selective attention to neutral distractors under load. *Psychophysiology*, 50, 398–406.
- Rossetti, H. C., Lacritz, L. H., Cullum, C. M., & Weiner, M. F. (2011). Normative data for the Montreal cognitive assessment (MoCA) in a population-based sample. *Neurology*, 77, 1272–1275.
- Salthouse, T. A. (1996). The processing-speed theory of adult age differences in cognition. *Psychological Review*, 103, 403–428.
- Seals, D. R., Justice, J. N., & LaRocca, T. J. (2016). Physiological geroscience: Targeting function to increase healthspan and achieve optimal longevity. *The Journal of Physiology*, 594, 2001–2024.
- Shao, Y. K., Mang, J., Li, P. L., Wang, J., Deng, T., & Xu, Z. X. (2015). Computer-based cognitive programs for improvement of memory, processing speed and executive function during age-related cognitive decline: A meta-analysis. *PLoS One*, 10, e0130831.
- Smith, S. M., Jenkinson, M., Woolrich, M. W., Beckmann, C. F., Behrens, T. E., Johansen-Berg, H., & Niazy, R. K. (2004). Advances in functional and structural MR image analysis and implementation as FSL. *NeuroImage*, 23, S208–S219.
- Thayer, J. F., Ahs, F., Fredrikson, M., Sollers, J. J., 3rd, & Wager, T. D. (2012). A meta-analysis of heart rate variability and neuroimaging studies: Implications for heart rate variability as a marker of stress and health. *Neuroscience and Biobehavioral Reviews*, 36, 747–756.
- Thayer, J. F., & Lane, R. D. (2000). A model of neurovisceral integration in emotion regulation and dysregulation. *Journal of Affective Disorders*, 61, 201–216.
- Woolrich, M. W., Jbabdi, S., Patenaude, B., Chappell, M., Makni, S., Behrens, T., & Smith, S. M. (2009). Bayesian analysis of neuroimaging data in FSL. *NeuroImage*, 45(1), S173–S186.
- Woutersen, K., Guadron, L., van den Berg, A. V., Boonstra, F. N., Theelen, T., & Goossens, J. (2017). A meta-analysis of perceptual and cognitive functions involved in useful-field-of-view test performance. *Journal of vision*, 17(14), 11.
- Ye, L., & Keogh, E. (2010). Time series shapelets: A novel technique that allows accurate, interpretable and fast classification. *Data Mining and Knowledge Discovery*, 22, 149–182.
- Ye L., & Eamonn, K. 2009. Time series shapelets: A new primitive for data mining. *Proceedings of the 15th ACM SIGKDD international conference on knowledge discovery and data mining*: pp. 947–56.
- Zahn, D., Adams, J., Krohn, J., Wenzel, M., Mann, C. G., Gomme, L. K., ... Kubiak, T. (2016). Heart rate variability and self-control—A meta-analysis. *Biological Psychology*, 115, 9–26.

SUPPORTING INFORMATION

Additional supporting information may be found online in the Supporting Information section at the end of this article.

How to cite this article: Chen Q, Yang H, Rooks B, et al. Autonomic flexibility reflects learning and associated neuroplasticity in old age. *Hum Brain Mapp*. 2020;41: 3608–3619. <https://doi.org/10.1002/hbm.25034>